Biometals (2022) 35:1059–1076
https://doi.org/10.1007/s10534-022-00422-4

Copper(II) cation and bathophenanthroline coordination enhance therapeutic effects of naringenin against lung tumor cells

Janetsi Y. Caro-Ramírez · María G. Rivas · Pablo J. Gonzalez · Patricia A. M. Williams · Luciana G. Naso · Evelina G. Ferrer

Received: 24 March 2022 / Accepted: 18 July 2022 / Published online: 5 August 2022

Abstract The development of new anticancer compounds is one of the challenges of bioinorganic and medicinal chemistry. Naringenin and its metal complexes have been recognized as promising inhibitors of cell proliferation, having enormous potential to act as an antioxidant and antitumorigenic agent. Lung cancer is the second most commonly diagnosed type of cancer. Therefore, this study is devoted to investigate the effects of Cu(II), naringenin (Nar), binary Cu(II)-naringenin complex (CuNar), and the Cu(II)-naringenin containing bathophenanthroline as an auxiliary ligand (CuNarBatho) on adenocarcinoma human alveolar basal epithelial cells (A549 cells) that are used as models for the study of drug therapies against lung cancer. The ternary complex shows selectivity being high cytotoxic against malignant cells. The cell death generated by CuNarBatho involves ROS production, loss of mitochondrial membrane potential, and depletion of GSH level and GSH/GSSG ratio. The structure-relationship activity was assessed by comparison with the reported Cu(II)-naringenin-phenanthroline complex. The CuNarBatho complex was synthesized and characterized by elemental analysis, molar conductivity, mass spectrometry, thermogravimetric measurements and UV–VIS, FT-IR, EPR, Raman and ^{1}H-NMR spectroscopies. In addition, the binding to bovine serum albumin (BSA) was studied at the physiological conditions (pH = 7.4) by fluorescence spectroscopy.

Supplementary Information The online version contains supplementary material available at https://doi.org/10.1007/s10534-022-00422-4.

J. Y. Caro-Ramírez · P. A. M. Williams (✉) · L. G. Naso · E. G. Ferrer (✉)
Centro de Química Inorgánica (CEQUINOR, UNLP, CONICET, asociado a CICPBA), Departamento de Química, Facultad de Ciencias Exactas, Universidad Nacional de La Plata, Bv. 120 N° 1465 La Plata, CP 1900 Buenos Aires, Argentina
e-mail: williams@quimica.unlp.edu.ar

E. G. Ferrer
e-mail: evelina@quimica.unlp.edu.ar

M. G. Rivas · P. J. Gonzalez
Departamento de Física, Facultad de Bioquímica Y Ciencias Biológicas, Universidad Nacional del Litoral and CONICET, S3000ZAA Santa Fe, Argentina

Graphical abstract

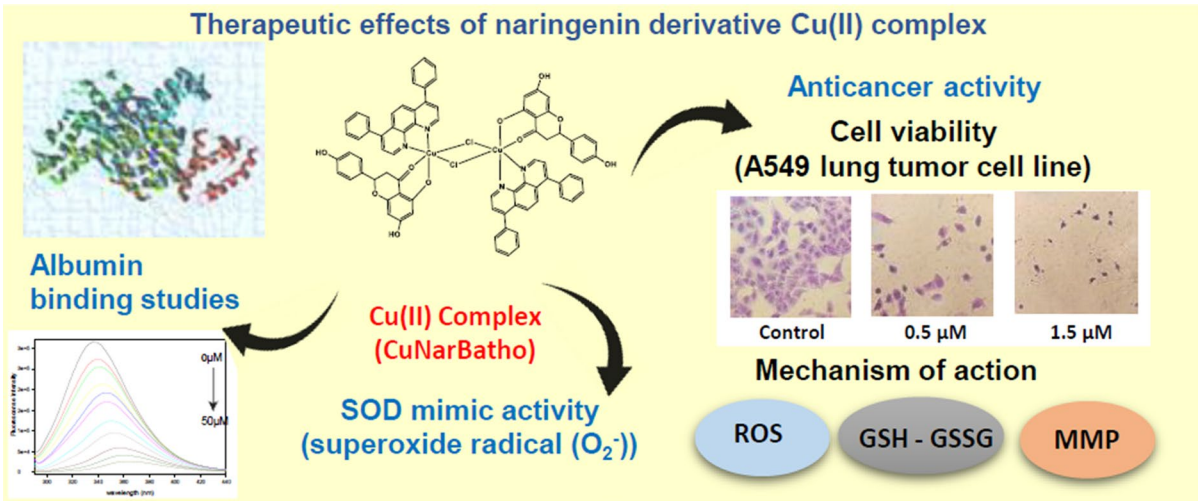

Keywords Copper(II) · Bathophenanthroline · Naringenin · Anticancer activity · Albumin interaction

Introduction

According to estimates from the World Health Organization (WHO) in 2019, cancer is the first or second leading cause of death before the age of 70 years in 112 of 183 countries. Lung cancer is the second most diagnosed cancer and the leading cause of cancer death in 2020, representing approximately 11.4% of diagnosed cancers and 18.0% of deaths. (Sung et al. 2021) The development of new anticancer compounds is one of the challenges of bioinorganic and medicinal chemistry. Although cisplatin is an effective chemotherapeutic drug, the drug resistance and numerous undesirable side effects limit its use in cancer treatment (Dasari and Tchounwou, 2014). In this sense, a new class of nonplatinum metal complexes such as copper and ruthenium-based complexes shows encouraging perspectives. Casiopeinas® are efficient anticancer agents with the general formula $[CuL^1L^2H_2O]NO_3$ where L^1 is an aromatic diimine-type ligand (N–N) and L^2 is a bidentate α-aminoacidate (N–O) or oxygen-only donor (O–O) ligand. Among them, Casiopeina III-ia, has completed preclinical trials and clinical phase I studies to treat leukemia have been started (Ruiz-Azuara et al. 2014). Likewise, there are reports of Ru-based compounds which are in the clinical phase for the potential cancer treatment. Among the Ru-based complexes, only Ru(III)-based drug NKP-1339 has started phase-Ib clinical trials for colorectal cancer treatment (Mahmud et al. 2021). Naringenin (4′,5,7-Trihydroxyflavanone) (chemical structure in Scheme 1), is a flavanone that can be extracted from citrus fruits such as lemon, grapefruit, and orange. Like other flavonoids, naringenin has low water solubility and stability being able to exert different biological effects. (Patel et al. 2018) Flavonoids can be modified by complexation with metals including copper(II) in order to improve their drug pharmaceutical activity or reduce their toxic effects. In particular, Cu(II)-naringenin complex (CuNar) showed a moderate inhibitory rate (*ca*. 30%) against HepG2 cell line (Tan et al. 2009). The introduction of diimine ligands in the coordination sphere of the complexes allows the increase of lipophilicity which could improve the cellular uptake. The cytotoxic activity of two ternary Cu(II)-naringenin complexes with 1,10-phenanthroline and 2,2′-bipyridine as coligands against A549 cell line was reported. Both compounds enhanced the anticancer activity of the free ligands

Scheme 1 Feasible CuNar-Batho synthesis pathway

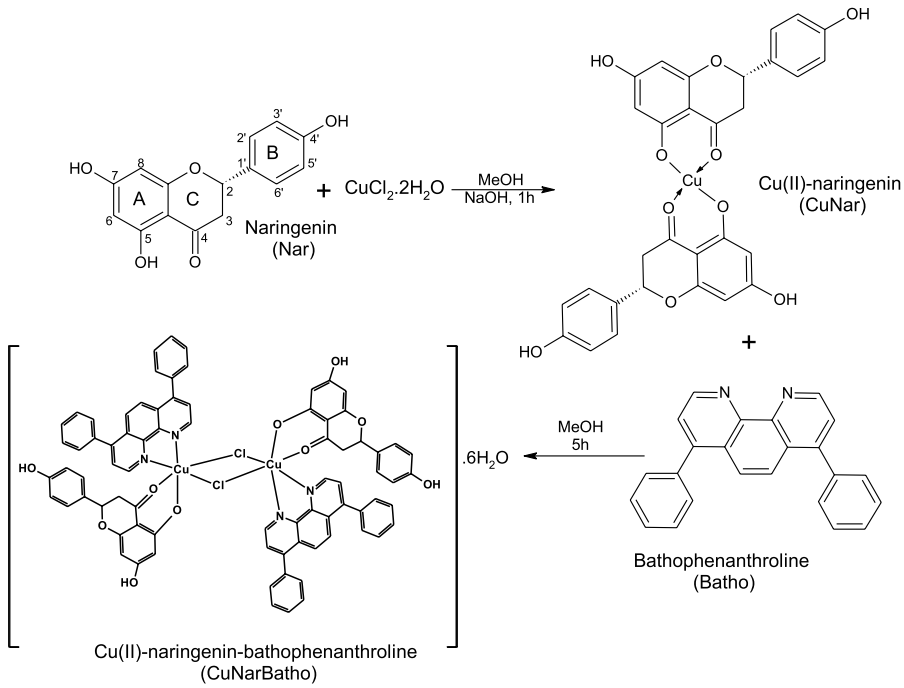

being their IC_{50} values < 50 µM. (Tamayo et al. 2016; Filho et al. 2014) On the other hand, 4,7-diphenyl-1,10-phenanthroline (Bathophenanthroline, Batho) is another of the most common N–N chelating ligands used in coordination chemistry. Due to the presence of aromatic rings in its structure, it can be inserted between paired DNA bases through π-π stacking improving the biological properties of the compounds (Shahabadi et al. 2013). The cytotoxic activity of Cu(II)-pomiferin-Batho complex, on several cancer cell lines, was published by Vančo et al. (Vančo et al. 2021) The complex behaved as an effective antiproliferative agent, with IC_{50} values of 2.6–22.9 µM, and its probable cell death mechanism involved the initiation or progression of oxidative stress. (Vančo et al. 2021) In the present work, we have synthesized and characterized a mixed ligand complex of Cu(II) containing naringenin as main ligand and bathophenanthroline as auxiliary ligand. In addition, the anticancer activity of the ternary complex against A549 cell line was evaluated and its probable mechanism of action was studied by means of cellular reactive oxygen species (ROS) generation, GSH levels depletion, and mitochondrial membrane potential determination. For comparative purposes, the A549 cell viability for the binary CuNar complex was also included. In addition, antioxidant activity (SOD mimic) and the interaction of the ternary complex with bovine serum albumin (BSA) were investigated.

Materials and Methods

Naringenin (Sigma), bathophenanthroline (Sigma) and copper(II) chloride dihydrate (Anedra), were used as supplied. Corning or Falcon provided tissue culture materials. Dulbecco's modified Eagle's medium (DMEM) was purchased from Gibco (Gaithersburg, MD, USA), Tryple™ from Invitrogen (Argentina SRL) and fetal bovine serum (FBS) from Internegocios, Argentina. All other chemicals used were of analytical grade. Elemental analysis for carbon, nitrogen and hydrogen was performed using a Carlo Erba EA1108 analyzer. Thermogravimetric analysis was performed with Shimadzu systems (model TG-50), working in synthetic air flow of 50 $ml.min^{-1}$ and at a heating rate of 10 $°C.min^{-1}$. Sample quantities ranged between 10 and 20 mg. UV–Vis spectra were recorded on a Hewlett-Packard 8453 diode-array and a Shimadzu 2600/2700 spectrophotometer. Infrared spectra were measured with a Bruker IFS 66 FTIR spectrophotometer from 4000 to 400 cm^{-1} using the KBr pellet technique. Raman spectra were collected on a Raman Horiba Jobin Yvon T64000 (confocal

microscopy Olympus BX41) spectrophotometer with a laser power of 100–10 mW and a spectral resolution of 4 cm^{-1}. Each spectrum was obtained as an average of 10 scans collected in the 1700–135 cm^{-1} range. Fluorescence spectra were obtained with a Shimadzu RF-6000 spectrophotometer equipped with a pulsed xenon lamp. The molar conductance of the complex was measured on a Conductivity TDS Probe—850084, Sper Scientific Direct, using 10^{-3} M DMSO and DMSO:H_2O solutions. Mass spectra were obtained using a Bruker micrOTOF-Q II mass spectrometer, equipped with an ESI source operating in positive mode. The experimental procedure involved the addition of 0.05% of formic acid. X and Q band CW-EPR spectra of both powder samples and frozen solutions were recorded at 120 K on a Bruker EMX-Plus spectrometers equipped with a rectangular cavity, with 100 kHz modulation frequency, 10 G modulation amplitude, and 2 mW microwave power. The spectra were baseline corrected using WinEPR Processing software (Bruker, Inc) and simulations were performed using the EasySpin 5.2.3 toolbox based on MATLAB. (Stoll and Schweiger 2006). X-ray powder diagram was recorded with a PANalytical X'Pert Pro automatic diffractometer with a scintillation detector and a graphite output monochromator using CuKα radiation (λ = 1.5406 Å). The PXRD data were collected in the $10° \leq 2\theta \leq 50°$ range, with 0.02° step width and 5 s counting time per step. A Bruker Ultrashield 600, 14.1 Tesla spectrometer was used for ^{1}H-NMR measurements, working with 100% DMSO-d6 solution (0.01 M concentrations) at 25 °C. Tetramethylsilane was used as internal standard for calibrating chemical shift δ.

Chemistry: Synthesis of Cu(II)-Naringenin-Bathophenanthroline complex (CuNarBatho)

In the beginning, 0.25 mmol (0.0681 g) of naringenin (Nar) was dissolved in 10 ml of methanol. To this solution, 250 µl of a 1 M sodium hydroxide solution was added raising the pH of the solution to ~ 11 $\left({}^{S}_{w}\mathrm{pH} = 9, {}^{S}_{S}\mathrm{pH} - 11\right)$ (Gibson et al. 2006) The mixture was kept in constant agitation, and an equimolar solution of $CuCl_2$ in methanol (0.25 mmol, 0.0426 g, 5 ml) was added dropping to acidic pH value $\left({}^{S}_{w}\mathrm{pH} = 3, {}^{S}_{S}\mathrm{pH} - 5\right)$. Immediately after, a green precipitate was observed (during the preparation, it has been verified by FTIR spectroscopy that this solid corresponded to the CuNar binary complex). The reaction was continued for an hour under agitation at room temperature. After that, a methanol solution containing bathophenanthroline (0.25 mmol, 0.0831 g, 5 ml) was slowly added and the agitation continued for 5 h. Over time, the color of the reaction changed, and a green apple precipitate was formed. The solid was filtered under vacuum, washed several times with methanol and water, and allowed to dry on the stove oven at 60 °C.

Anal. Calc. for $C_{78}H_{66}N_4O_{16}Cl_2Cu_2$ (1513.38 g/mol) %: Calc. C, 61.90; H, 4.40; N, 3.70, Cl, 4.69. Found. C, 61.88; H, 4.30; N, 3.68, Cl, 4.71. ESI–MS: experimental: m/z 666.13 theoretical m/z 666.12 ($C_{39}H_{27}N_2O_5Cu^+$, Fig S1). Thermogravimetric study (synthetic air, flow: 50 ml/min, heating rate: 10 °C/min) confirmed the presence of six labile water molecules (Exp. loss: 7.04%. Calc. loss: 7.14%), corresponding to the CuNar-Batho ($[CuNarBathoCl]_2.6H_2O$) complex (Fig. S2). Diagnostic powder diffraction peaks at unique 2θ-values (in degrees) of 14.10, 16.69, 19.39, 24.67, 25.48, 26.81 (Fig. S3). UV–Vis spectra: solution (DMSO): 645 nm ($\varepsilon = 190$ M^{-1} cm^{-1}), 290 nm ($\varepsilon = 76.000$ M^{-1} cm^{-1}); solid spectrum: 642, 350 nm (sh), 297 nm y 224 nm. Molar conductivity: 1 mM, DMSO at 25 °C: 12 $\Omega^{-1}.cm^2.mol^{-1}$.

Albumin interaction

Interaction of the complex with BSA was measured by fluorescent technique. BSA solution (6 µM) in Tris–HCl buffer (0.1 M, pH = 7) was maintained constant and different concentrations of the complex ranging from 2 to 50 µM (incubation time = 1 h) were added. The effects of the complex on the quenching of the emission intensity of BSA at 340 nm was examined at $\lambda_{ex} = 280$ nm at three different temperatures 298, 303 and 310 K. Inner-filter effect was taken into account and fluorescence intensities were corrected using the following equation $F_{corr} = F_{obs}$ x $e^{(1/2\ Aex\ +\ ½\ Aem)}$, where F_{corr} and F_{obs} are the fluorescence intensities corrected by inner-filter effect and recorded, respectively, A_{ex} and A_{em} are the electronic absorbances of the solutions at excitation and emission wavelengths, respectively. (Lakowicz 2013)

Three independent replicates were performed for each sample and concentration.

Superoxide dismutase activity

In this method, the generation of the superoxide radical anion was realized by the system phenazine methosulfate (PMS)/nicotinamide adenine dinucleotide, reduced (NADH). The system included: 1.5 mM NADH (0.125 ml), 300 µM of nitrobluetetrazolium (NBT, 0.125 ml) in a phosphate buffer (pH 7.4, 0.1 M) solution and sample (0.125 ml). The mixture was incubated for 15 min at 25 °C, and the reaction started with the addition of PMS (0.125 ml, 120 µM). The solutions of the compounds were prepared in DMSO (except bathophenanthroline which was dissolved in ethanol) before adding the phosphate buffer to achieve the required final concentrations. Then, the reaction mixture was incubated for 5 min at 25 °C. The reaction was followed by UV–Vis spectroscopy monitoring the absorbance at 560 nm. The amount of compound that produced a 50% inhibition of NBT reduction is obtained by plotting the percentage of inhibition versus sample concentration. The constant value (k), which is independent of both detector concentration and nature, is calculated according to: $k_{McCF} = k_{detector}$x[detector]/IC_{50}(sample), where k_{NBT} (pH 7.8) = 5.94×10^4 $mol^{-1}xLxs^{-1}$ and [detector] = detector concentration.

Cell culture

Human lung carcinoma cell line A549 was cultured in Dulbecco's Modified Eagle Medium (DMEM) supplemented with 10% fetal bovine serum (FBS), penicillin (100 U/ml) and streptomycin (100 µg/ml) in a humidified 37 °C incubator with atmosphere of 5% CO_2. When 70–80% confluence was reached, cells were washed with phosphate buffered saline (PBS) (11 mM KH_2PO_4, 26 mM Na_2HPO_4, 115 mM NaCl, pH 7.4) and were subcultured using TrypLE™. For the experiments, cells were grown in multi-well plates. When cells reached 70% confluence, the monolayers were washed twice with DMEM and then incubated with different compounds.

Analysis of cell viability

To evaluate the cytotoxicity of compounds, MTT (3-(4, 5-dimethylthiazol-2-yl)-2, 5-diphenyl-tetrazolium bromide) assay was performed and cell viability was determined. Briefly, A549 cells were seeded at a density of 2×10^5 per well in a 96-well for 24 h. Then, cells were treated with naringenin, bathophenantroline, CuNar or CuNarBatho at different concentrations for additional 24 h. Each concentration was repeated three times. After the exposure period, the medium was removed and the cells were washed with PBS and incubated with MTT solution (0.5 mg/ml) (Sigma, St. Louis, MO, USA) for 2 h. Afterwards, the medium was removed and the viable cell number per dish (directly proportional to the production of formazan which was solubilized in DMSO) was measured spectrophotometrically at 560 nm. The percentage of viable cells was estimated by comparing with the untreated control cells.

Intracellular reactive oxygen species (ROS) generation

Intracellular reactive oxygen species (ROS) generation in A549 cell line was measured by oxidation of 2′,7′-dichlorodihydrofluorescein diacetate (H_2DCFDA) to 2′,7′-dichlorofluorescein (DCF). Briefly, 24-well plates were seeded with 5×10^4 cells per well and allowed to adhere overnight. Then, different concentrations of compounds were added for 3 (only CuNarBatho) and 24 h. Then, media was removed, and cells were loaded with 10 µM H_2DCFDA diluted in clear media for 30 min at 37 °C. Media was then separated and the cell monolayers rinsed with PBS and lysated into 1 ml 0.1% Triton-X100. The cell extracts were then analyzed for the oxidized product DCF by fluorescence spectroscopy (excitation wavelength, 485 nm; emission wavelength, 535 nm). (Ling et al. 2011).

Cell morphology

To evaluate morphological changes cells were grown in six well per plates and incubated 24 h with fresh serum-free DMEM without (control) or with different concentrations of the complex. The monolayers

were subsequently washed twice with PBS, fixed with methanol and stained with violet crystal for 10 min. Then, they were washed with water and the morphological changes were examined by light microscopy.

Determination of mitochondrial membrane potential

For the determination of mitochondrial membrane potential (MMP), cells were treated with the compounds, washed with PBS and stained with 0.4 nM of 3,3′-dihexyloxacarbocyanine iodide, $DiOC_6$ (40 nM stock concentration in DMSO). Changes in MMP ($\Delta\Psi m$) were measured using a fluorometer Shimadzu RF 6000 (excitation/emission = 488 nm/525 nm). (Akkoç et al. 2015).

GSH assay

For GSH determinations, 100 µl aliquots of cells after 24 h incubation with the compounds were mixed with 1.8 µl of ice-cold phosphate buffer (Na_2HPO_4 0.1 M-EDTA 0.005 M, pH 8) and 100 µl ophthaldialdehyde (OPT) (0.1% in methanol) as it was described by Hissin and Hilf (1976). For GSSG determinations, 100 ml aliquots were mixed with 1.7 µl NaOH 0.1 M and OPT but previously, and to avoid GSH oxidation, the cellular extracts for GSSG determination were incubated with 0.04 M of N-ethyl-maleimide (NEM). The fluorescence λ_{em} 420 nm was determined (λ_{ex} 350 nm). The protein content in each cellular extract was quantified using the Bradford assay. (Bradford 1976).

Statistical analysis

Statistical analyses were evaluated using the analysis of variance method (ANOVA) followed by the test of least significant difference (Fisher). Statistical significance was defined as $p < 0.05$.

Results and discussion

Chemistry and physicochemical characterization

To improve the anticancer activity of copper(II) naringenin complex, a ternary complex using bathophenanthroline as co-ligand was obtained. To a mixture containing naringenin at $^{S}_{S}$pH − 11 (Scheme), a methanolic solution of $CuCl_2$ was added lowering the $^{S}_{S}$pH − 5 forming the binary CuNar complex. Over time and after the addition of bathophenanthroline, the ternary complex was formed and precipitated as a solid of apple green color. Unfortunately, all the experiments carried to obtain crystals did not succeed. Nonetheless, the complex was fully characterized by several physicochemical techniques.

The elemental analyses and molar conductivity suggested that the formula of the complex agrees with a 1:1:1 Nar:Batho:Cu(II) stoichiometry and that the complex in DMSO solution is a non-electrolyte (Table S1). Thermogravimetric determinations suggested the presence of six water molecules (Fig. S2). The compound is soluble in DMSO (2 mg/ml at 20 °C and 10 mg/ml at 37 °C), and in the DMSO/H_2O mixtures (biological assays) and moderately soluble in DMF and DMA having low solubility in polar solvents (water, methanol, ethanol, acetonitrile).

The ESI–MS of the complex was also investigated in DMSO:H_2O (1:10) solution containing 0.05% of formic acid, and the most relevant peaks are shown in Fig. S1. The characteristic peak observed at m/z 666.13 (100.0%), together with their appropriate isotopic pattern (line-to-line separation of 1), could be assigned to the mononuclear complex with bathophenanthroline and naringenin ligands (Cu(II)(Nar-H)Batho$^+$, $C_{39}H_{27}N_2O_5Cu^+$). Mono-charged species containing Cu(II) or Cu(I) were found. Reduction processes have been observed in Cu(II) solutions as well as species derived from recombination or fragmentation occurring in the experiment (Pivetta et al. 2015; Gençkal 2020; Northcote-Smith et al. 2021). Thus, other fragmentation major species were identified as Cu(II)(Batho)(formate)$^+$ (11.4%, m/z 440.07), Cu(II)$(Batho)_2Cl^+$ (22.0%, m/z 762.17) and Cu(I)$(Batho)_2^+$ (9.1%, m/z 727.20). All of those with a line-to-line separation of unity. Other relevant signals were assigned to isotopically related species.

Additionally, the coordination of copper(II) with the ligands was assessed via ^{1}H-NMR Spectra, EPR, FTIR, Raman and UV–Vis spectra.

The ^{1}H-NMR spectrum obtained from the complex is shown in Fig. S4. To perform the comparison, it was superimposed with the calculated spectra of naringenin and bathophenanthroline (MestReNova@). As it is known, naringenin has a keto group at C-4 and lacks the 2,3-olefinic bond. Thus, it can act as a

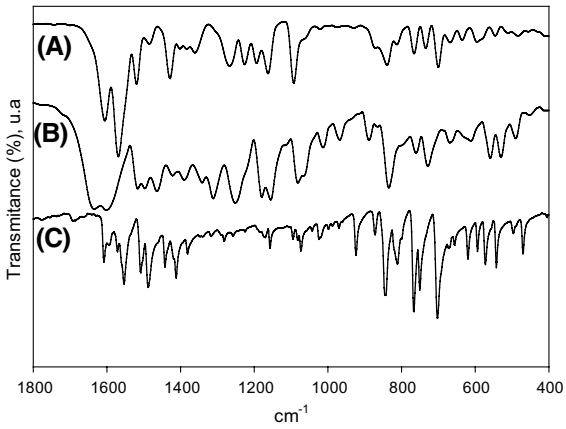

Fig. 1 FTIR spectra of **A** CuNarBatho, **B** naringenin, **C** bathophenanthroline. (2000–400 cm^{-1} region)

bidentate ligand for metals through the 5-alkoxide ion and the 4-keto group. In addition, it possesses two differentiable OH groups at positions 7 and 4′ (Fig. S4). These OH groups display ^{1}H-NMR signals at 12.15 ppm (5-OH), 10.79 ppm (7-OH), and 9.59 ppm (4′-OH), respectively (Celiz et al. 2019). On the other hand, bathophenanthroline shows a group of signals compressed in the 7.4–8.8 ppm range (Fig. S4). Is it usual, that the ^{1}H-NMR of the metal complex appeared with broad signals explained by the presence of the paramagnetic copper atom, the loss of the flavonoid planarity, and the decrease of the electrons mobility (Fig. S4)(Pereira et al. 2007). Nevertheless, it is noted the absence of the proton located around 12.15 ppm (5-OH) while the corresponding signals to 7-OH (10.73 ppm) and 4′-OH (9.51 ppm) were observed. This result suggested the presence of an alkoxide group in the complex and that the other hydroxyl groups are not involved in the coordination with the metal center. In addition, a broad band with a maximum of 7.58 ppm generated from the coordination with the copper(II) center, was assigned to bathophenanthroline. In this region the proton signals of the N,N-ligand are expected and no bands of naringenin were observed (Fig. S4).

The FTIR spectrum of the complex showed bands suggesting coordination to the metal (Fig. 1). The characteristic νC4 = O stretching band of naringenin at 1633 cm^{-1} was shifted to 1605 cm^{-1} with the formation of the complex. The $\Delta\nu$ is 28 cm^{-1} suggesting a coordination bond with the metal. (Wang et al. 2006) In addition, the band around 3200 cm^{-1} (sh) due to phenolic hydroxyl in the free ligand showed a significant change in the copper complex, observed at 3240 cm^{-1}, being probably related to the formation of chelates through the deprotonated 5-hydroxyl group. This change correlated with the modification observed of the 1600 cm^{-1} band (δ 5-OH and 7-OH) of the naringenin. Supporting the interaction through the deprotonated 5-OH group, the band located at 1314 cm^{-1} (δC-5OH) disappeared in the complex. (Celiz et al. 2019) The broad band around 3400 cm^{-1} could be associated with the presence of water molecules confirmed by

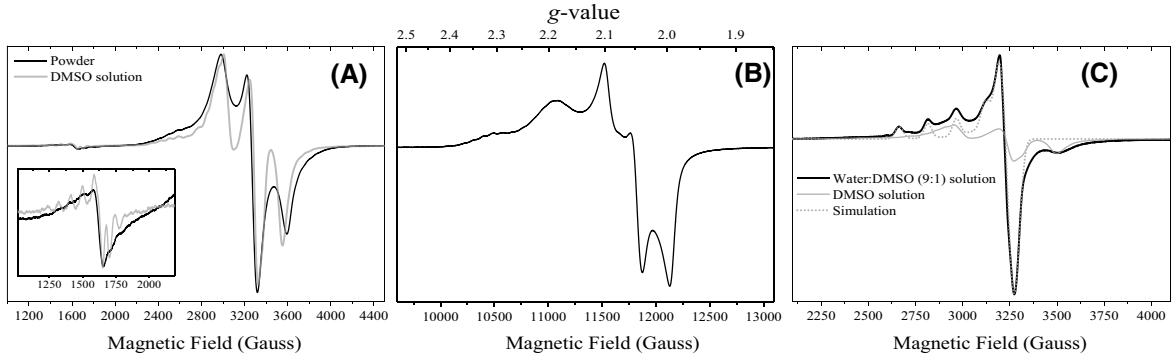

Fig. 2 **A** X-band EPR spectra obtained at 120 K, 10 G modulation amplitude, 2 mW microwave power. For a powdered sample (black line) and DMSO solution (gray line) of CuNarBatho dimer. Inset shows the half-field ΔMs = ±2 transition. **B** Q-band EPR spectra obtained at 298 K, 10 G modulation amplitude, 1 mW microwave power for a powdered sample. **C** EPR spectrum of H_2O:DMSO (9:1) (Black) solution superimposed with that of the dimer in DMSO solution (gray) and the simulation of H_2O:DMSO (9:1) solution spectra (dot line)

TGA thermal studies (Tamayo et al. 2016) Moreover, the $\nu C=C$ aromatic stretching band moved to 1570 cm^{-1} in the complex.

The bathophenanthroline characteristic bands were observed at 766, 734, 700 y 635 cm^{-1}. Those bands did not appear in the binary CuNar complex. Bands located at 545 cm^{-1} and 456 cm^{-1} could be additionally indicative of the interaction of the ligand with the metal, being tentatively assigned at νCu-O and νCu-N stretching vibrational modes. (Ramos et al., 2014). In addition, the Raman spectrum of CuNarBatho was analyzed and compared with the spectra of the Batho, Nar and CuNar to evaluate the coordination mode of the chloride ligand through the determination of the presence of $\nu(Cu\text{-}Cl_{terminal})$ stretching or the presence of the bridge mode ν(M-Cl-M), because both types of vibrational modes appear out of the FTIR measurement range (Fig. S5). The absence of the band at 320–350 cm^{-1} region ($\nu(Cu\text{-}Cl_{terminal})$) and the observation of the band at 150 cm^{-1} associated with chloro-bridge symmetric vibration only for CuNarBatho complex suggested the presence Cu-Cl-Cu bonds (Litos et al. 2007; Joseph et al. 2006). These results are consistent with the coordination of copper(II) ion through the 5-alkoxy and 4-keto groups of the naringenin and the nitrogen atoms of bathophenanthroline ancillary ligand.

To gain a deeper insight into the structure of the complex, EPR studies were undertaken. The EPR spectra of both powder and frozen DMSO solution of CuNarBatho are shown in Fig. 2A. Both powder (Fig. 2A, black) and DMSO solution (Fig. 2A, gray) spectra are typical of a magnetic copper dimer, where the two interacting paramagnetic Cu(II) ions ($S_1=S_2=1/2$) can be described by a phenomenological spin Hamiltonian ($\hat{\mathbf{H}}=\hat{\mathbf{H}}_{\mathbf{Z}}+\hat{\mathbf{H}}_{\mathbf{hf}}+\hat{\mathbf{H}}_{\mathbf{J}}+\hat{\mathbf{H}}_{\mathbf{ZFS}}$) that contains all the interactions between electron spins $\mathbf{S_1}$ and $\mathbf{S_2}$ with the external magnetic field $\mathbf{B_0}$ (Zeeman interaction, $\hat{\mathbf{H}}_{\mathbf{Z}}$), the nuclear spins $\mathbf{I_1}$ and $\mathbf{I_2}$ of both copper ions (hyperfine interaction, $\hat{\mathbf{H}}_{\mathbf{hf}}$), and the exchange interaction (isotropic and dipolar, $\hat{\mathbf{H}}_{\mathbf{J}}+\hat{\mathbf{H}}_{\mathbf{ZFS}}$) (Rizzi et al. 2016). The spectral features of both powder and frozen DMSO solution indicate that $\hat{\mathbf{H}}_{\mathbf{Z}}>\hat{\mathbf{H}}_{\mathbf{ZFS}}$ at X-band, as the allowed ($\Delta Ms=\pm1$) and one forbidden weak transition at half-field ($\Delta Ms=\pm2$, *ca.* 1630 Gauss) are clearly observable. Additionally, both the solid complex and DMSO frozen solution showed a central line at ca. 3200 Gauss. The intensity versus temperature plots (Fig. S6) of the EPR lines of both the dimer and the central line indicated that, the feature observed at ~ 3200 Gauss is originated neither from double-quantum transitions nor collapse (U-peak) (Calvo et al. 2017), but instead, it might correspond to magnetically isolated Cu(II) ions generated as a synthesis by-product or by degradation of the dimer.

The Q-band powder spectrum (Fig. 2B) obtained at room temperature (298 K) showed increased resolution of some spectral components and, in agreement with the relation developed by Eaton et al., a half-field transition almost undetectable (Eaton et al. 1983). The observed hyperfine interaction of ~ 95 Gauss of both electron spins (S_1 and S_2) with both copper nuclear spins ($n=2$, $I=3/2$) is detectable at both X- and Q-band (Fig. 2A and 2B), as some spectral features are split into $[2nI+1]=7$ lines. A simulation of the X-band powder spectrum yielded the values $g_{\parallel}=2.200$; $A_{\parallel}=95$ Gauss; $D=0.050$ cm^{-1}. Using the simulated spectrum and relationship developed by Eaton et al., between the ratio of the intensities of each transition ($I_{\Delta Ms=2}$ / $I_{\Delta Ms=1}$, each one determined as the double-integral) and r^{-6}, the intradimer inter-spin distance can be estimated (Eaton et al. 1983). This analysis indicates that the Cu-Cu distance is ~ 3.7 Å.

Since the population of the singlet and triplet states is governed by the Boltzmann distribution and the Curie law according to $[Intensity]=(3/T)\times(\exp(-J/k_BT))$, the isotropic exchange interaction constant (J) was estimated to be ~ 30 K (21 cm^{-1}) by studying the variation of EPR signal intensity versus absolute temperature (Aboukais et al. 1992). The calculated distance and the estimated J value agreed with the presence of halogen bridges between the copper centers (Teipel et al. 1994).

On the other hand, the EPR spectrum of the DMSO:H_2O solution measured at 120 K shows mainly the typical spectrum for a magnetically-isolated axial Cu(II) ion (Fig. 2C, black). Spectral analysis indicates that some of the dimer is still present (Fig. 2C, gray). This result indicates that water break up the copper dimer. The simulation performed with a spin Hamiltonian for an isolated Cu(II) ion ($\hat{\mathbf{H}}=\hat{\mathbf{H}}_{\mathbf{Z}}+\hat{\mathbf{H}}_{\mathbf{hf}}$) yields $g_z=2.298$, $g_y=2.069$, $g_x=2.042$, $A_z=170$ G (0.0182 cm^{-1}). This essentially axial spectrum with $g_{\parallel}>g_{\perp}>g_e=2.0023$ is expected for tetragonal and related square-planar geometries. The highly axial hyperfine interaction with the $I=3/2$

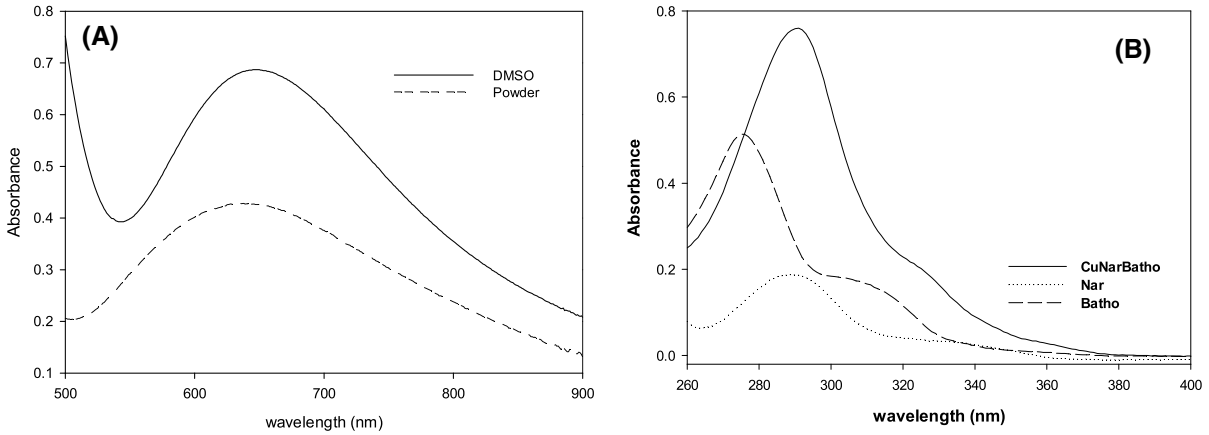

Fig. 3 **A** Solid and solution DMSO (3.5 mM) spectra of CuNarBatho complex (500–900 nm region), **B** Solution spectra in the 260–400 nm range of CuNarBatho complex (DMSO, 10 μM), bathophenanthroline (10 μM, %DMSO = 99.8%) and naringenin (DMSO, 10 μM)

of $^{63/65}$Cu nucleus is manifested as the splitting into four lines of the $g_{\|}$ resonance only. In addition, these parameters fit well in the corresponding $g_{\|}$ vs. $A_{\|}$ diagram for a the expected 2N2O coordination sphere. (Peisach and Blumberg 1974).

UV–Vis studies were measured both in the solid-state and in solution (Fig. 3A). Solid spectra showed at 642 nm the characteristic d-d transition band of the Cu(II) ion. In the DMSO solution, the d-d band shifted to higher wavelengths, 645 nm ($\varepsilon = 190$ M^{-1} cm^{-1}, 3.5 mM). This displacement is probably due to the solvent effect because in DMSO solution the complex remains as a dimer, as it could be determined by the EPR spectrum.

In the 400–260 nm region charge transfer bands can be observed. In the DMSO solution (Fig. 3B), naringenin showed two main absorption bands. The most intense band is located around 288 nm. According to Celiz et al. (Celiz et al., 2019), this band is related to the electronic transition over the A and C rings. The other band located at 316 nm was assigned to electronic $\pi \rightarrow \pi^*$ transition on the B ring. Bathophenanthroline also presented two bands in this region (Fig. 3B), one located at 275 nm and the other at 300 nm. At the same concentration values, the bands of the complex appeared at 290 nm and 318 nm with increased intensity compared with the bands of naringenin and bathophenanthroline. In H_2O:DMSO (99:1) solutions, at the same pH value and concentrations (pH = 7, 10 μM) (Fig. S7A) some differences can be observed. In addition to the marked difference in the intensity of the bands, in this media, the bands of the complex appeared at 286 and 315 nm showing a slight shift compared with both ligands taking an intermediate position between naringenin and bathophenanthroline ligands (289, 320 and 279 nm and 305 nm, respectively). For the flavonoid-copper complexes, these changes have been associated with the interaction of the Cu(II) ion with the 5-OH and C(4) = O positions of the condensed ring (Celiz et al 2019; Tan et al. 2009). Nevertheless, in the complex, both ligands are contributing with $\pi \rightarrow \pi^*$ transition bands in this region.

The chemical stability of the complex in DMSO:H_2O mixture (used for the biological assays) was investigated by UV–Vis spectroscopy during 24 h and the molar conductivity was measured at different time intervals (e.g. 5 min, Table S1) to estimate possible changes in the structure of the ternary complex. In the evaluation of the UV–Vis spectrum vs. time (Fig. S7B), it can be observed that the absorbance values were not appreciably modified, indicating its stability during 24 h.

In summary, in the solid complex, elemental analysis and conductivity data support the proposed stoichiometry. TGA measurements confirm the presence of six labile water molecules. Evidence of the binding mode of the ligands and their proposed structure were gathered from FTIR, Raman, diffuse reflectance, and EPR spectra. The FTIR spectrum supports the naringenin coordination through the 5-alkoxy and 4-keto groups and the nitrogen atoms

from bathophenanthroline around the copper(II) ion. This result is consistent with the 642 nm band of the diffuse reflectance spectrum. The ESI–MS spectrum shows a peak at m/z 666.13 (100.0%) corresponding to Cu(II)(Nar-H)Batho + specie. The NMR spectrum confirms the absence of the signal belonging to the 5-OH hydroxyl group suggesting the presence of the alkoxide group in the complex. EPR spectrum shows the presence of a dimer compound with the Cu-Cu distance of about 3.7 Å. The calculated distance and the *J* value agree with the existence of halogen bridges between the metal centers. The formation of other types of structures (e.g. paddle wheel) was discarded because of the expectation of shorter Cu..Cu distance (Mosae Selvakumar et al 2013) and a large type of exchange interaction. The presence of Cu–O-Cu type of bridges was additionally ruled out because they also require strong exchange interactions. The possibility of the presence of a chlorine bridge was considered. The Raman spectra of CuNarBatho were compared with the ligands and the binary CuNar. Only in the CuNarBatho complex a band related to νCu-Cl-Cu bridging motion was observed. This result allows us to suggest the dinuclear proposed structure in the solid complex (Scheme 1).

Additionally, for purposes of evaluation of the anticancer activity on lung cancer cells, the binary Cu(II)-naringenin complex (CuNar = $[CuNar_2(H_2O)_2]$) was prepared according to the method reported by Celiz et al. (Celiz et al., 2019) and data corresponding to the ternary CuNarPhen ($[Cu(H_2O)_2(Nar)(phen)](ClO_4)$) complex was taken from reference (Tamayo et al. 2016).

Albumin binding studies

Albumin binding experiments were carried out by fluorescence spectroscopy considering the intrinsic fluorescence of BSA. Its interaction may produce changes in the microenvironment of the protein resulting in a quenching of the characteristic BSA band located at 340 nm. This band is mainly generated by two tryptophan residues, Trp-134 in the first domain on the surface of the molecule and Trp-212 in the second domain, within a hydrophobic pocket and tyrosine. Tyrosine residue is also present with a lower contribution.

The modifications in this band depend on the environment of the Trp residues and their exposition in the side chain under the quencher interaction. The compound did not interfere with BSA fluorescence. The spectral changes of increasing CuNarBatho concentrations (0–50 μM) at 298 K are shown in Fig. 4A.

As the complex concentration increased, a remarkable decrease in the fluorescence intensity of BSA (> 90%) was observed together with a notorious bathochromic shift of the maximum emission wavelength from 340 to 363 nm. Those significant changes suggested strong complex-BSA interaction and a

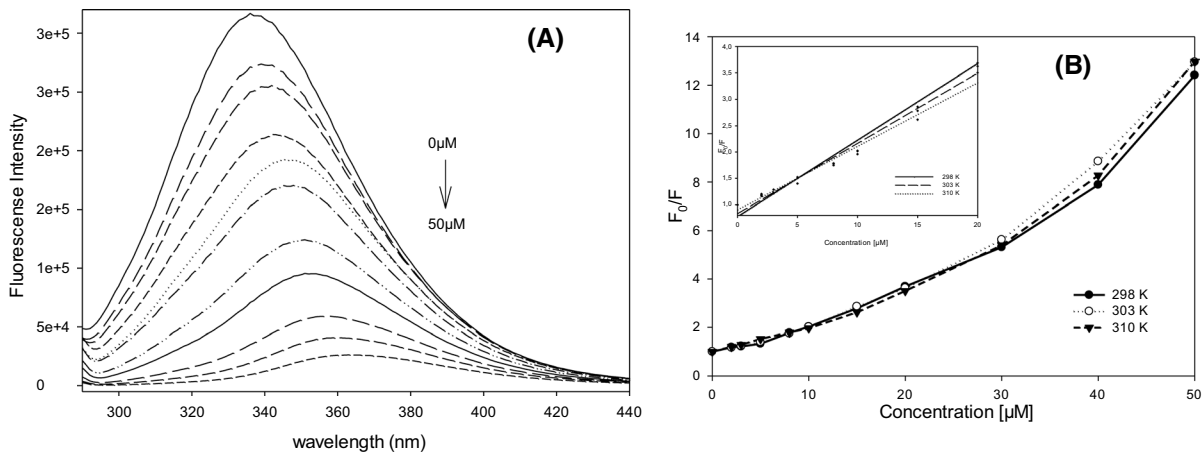

Fig. 4 **A** The fluorescence spectra of BSA in the presence of CuNarBatho complex at 298 K, $\lambda_{ex} = 280$ nm. The concentration of BSA was 6 μM, and the concentrations of the complex were 0, 2, 3, 5, 8, 10, 15, 20, 30, 40 and 50 μM, respectively; **B** Stern–Volmer plot for the binding of the complex to BSA (inset: 0–20 μM range)

Table 1 Stern–Volmer constant (K_{sv}), bimolecular quenching constant (K_q), binding constant (K_b) and number of binding sites (n) for the interaction of CuNarBatho with BSA (6 µM) in Tris–HCl buffer (0.1 M, pH 7.4). Naringenin data was added for comparative purposes. r^2 is the correlation coefficient

	T (K)	K_{sv} ($\times 10^4$) (M^{-1})	K_q ($\times 10^{12}$) ($M^{-1}.s^{-1}$)	r^2	K_b ($\times 10^5$) (M^{-1})	n	r^2
CuNarBatho	298	14.51 ± 0.66	14.51 ± 0.66	0.98	59.18 ± 0.16	1.35	0.99
	303	13.33 ± 0.72	13.33 ± 0.72	0.97	20.64 ± 0.06	1.26	0.99
	310	12.01 ± 0.66	12.01 ± 0.66	0.97	4.40 ± 0.17	1.12	0.98
Nar (Bi et al. 2012)	291	3.74 ± 0.05			0.41 ± 0.01	0.96	
	301	3.34 ± 0.09			0.40 ± 0.01	1.00	
	311	3.22 ± 0.03			0.39 ± 0.01	0.95	
Nar (Islas et al. 2015)	298	1.66 ± 0.08			1.02 ± 0.30	1.18	

Table 2 Thermodynamic parameters for CuNarBatho complex and naringenin

	ΔH (KJ mol^{-1})	ΔS (J $mol^{-1}K^{-1}$)	ΔG (KJ mol^{-1})
Nar*	−1.44	83.33	−25.69
CuNarBatho	−170.09	−440.67	−49.79

*Taken from reference (Bi et al. 2012)

conformational modification probably due to loss of the compact structure of hydrophobic sub-domain where tryptophan was located.

The fluorescence data was analyzed by the Stern–Volmer equation: $F_0/F = 1 + K_q\tau_0[Q] = 1 + K_{SV}[Q]$ where F_0 and F are the steady-state fluorescence intensities in the absence and presence of quencher, respectively. K_{SV} is the Stern–Volmer quenching constant and [Q] is the concentration of quencher. It was assumed: (i) the bimolecular quenching constant K_q equal to K_{SV}/τ_0, (ii) the lifetime of the fluorophore in the absence of the quencher as $\tau_0 = 1 \times 10^{-8}$ s (estimated value for a biopolymer) while Q is the quencher concentration (Nan et al. 2019). The plot F_0/F vs [Q] (Fig. 4B) showed positive deviation at the three temperatures. As it is known, the quenching mechanisms are classed as either dynamic quenching or static quenching. Both of them can be distinguished by their temperature dependency. For the static one, the quenching rate constants diminish with the increment of temperature, and a reverse effect is expected for dynamic quenching. This tendency can be distinguished by analyzing the Stern–Volmer graphs in the linear range (2 to 20 µM, Fig. 4B, inset) and obtaining the K_{SV} quenching constants values at different temperatures (Table 1). The values of K_{SV} indicated the presence of static quenching mechanism. The K_q values higher than the value of 1×10^{10} $M^{-1}.s^{-1}$ (diffusion-controlled quenching) reinforce this assumption. Thus, the binding constants and the number of binding sites can be obtained from the equation log $[(F_0\text{-}F)/F] = \log K_b + n \log [Q]$ (Table 1, Fig. S8) (Nan et al. 2019; Bi et al. 2012).

The K_b constant values at the three temperatures resulted in the order of 10^5 M^{-1}. The binding constant of the interaction of a compound with albumin must be high enough to ensure the transport and distribution throughout the organism but at the same time low enough so that the compound may be released to reach its target. The majority of the reversible-bound ligands have typical K_b values ranging from 10^4 to 10^6 M^{-1}. Additionally, the binding sites for the complex on BSA were approximately equal to unity, suggesting that there was one independent class of binding sites for this compound. Data reported for naringenin (Table 1) gave K_{sv} and K_b constants in the same order of magnitude but evidence that the complex interacts stronger than the free ligand.

The type of binding involved (H-bonding, Van der Waals, electrostatic, and hydrophobic interactions) can be elucidated from the thermodynamic parameters. The thermodynamic parameters (Table 2) were assessed using the Van't Hoff equation ($\ln K_b = -\Delta H/RT + \Delta S/R$) by plotting $\ln K_b$ vs 1/T (not shown) and the free energy changes (ΔG) were estimated from $\Delta G = \Delta H - T\Delta S$. The magnitudes and signs of these parameters may explain the main forces involved in the binding. The chosen temperatures were those

(298 K, 303 K and 310 K) in which the albumin does not suffer any structural degradation.

Table 2 shows the values obtained for the thermodynamic parameters. The interaction of naringenin, as well as the complex, resulted spontaneous in nature.

The difference in the interaction of Nar and CuNarBatho with BSA can be determined from the calculated ΔH and ΔS values. The negative ΔH and ΔS values for the complex suggest an enthalpic-driven process with Van der Walls and H-bond formation while naringenin seemed to be entropically driven mainly by hydrophobic associations.

Based on those results there is a great possibility that the complex could be transported for the albumin and turns out to be suitable for biological studies.

Biological studies

Antioxidant activity against superoxide radical (O_2^-)

Flavonoids are recognized for their antioxidant activities. There is a structure–activity relationship that recognizes that the absence of the hydroxyl group at position C3 in flavanones and the absence of the catechol structure in the B-ring leads to a decrease in their antioxidant capacity. In addition, and because flavonoids can capture free electrons through their hydroxyl groups, the presence of a C2 = C3 double bond also gives greater stability once the radical is formed. This prevents the spread of free radical chain reactions. This is the reason why naringenin, which does not contain the 3-OH group or the C2 = C3 double bond in its structure, is expected to have low antioxidant activity (Scheme). Previous work showed the lack of ability of naringenin to efficiently dismutate superoxide radical (Islas et al. 2015; Uivarosi and Munteanu 2017) and it has been demonstrated that flavonoids form metal complexes that usually are more potent antioxidants than the free ligands. Indeed, for naringenin Wang et al. (Wang et al. 2006)

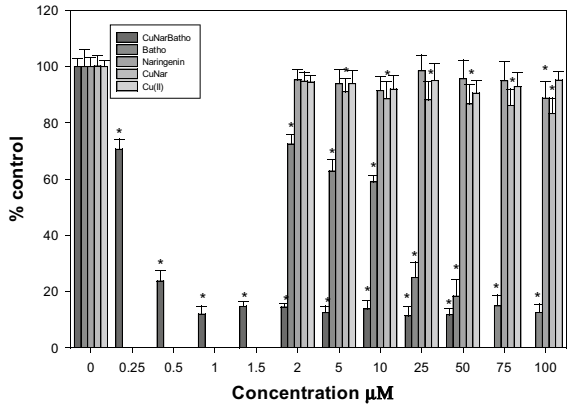

Fig. 5 Effects of naringenin, bathophenanthroline, CuNarBatho, CuNar, and copper(II) cation on A549 cell viability. Cells were plated in a 96-well plate and incubated with different concentrations (0.25 to 100 µM) of compounds for 24 h. Viable cells were estimated by MTT assay. Results are expressed as percent viability relative to control (untreated) cells. Data represents mean ± SD of three independent assays. Results were compared using ANOVA, followed by LSD analysis. *represent $p < 0.05$

showed that the binary CuNar complex can be a much better SOD mimic agent than the ligand, remarkably lowering the IC_{50} value (Table 3) The lack of SOD activity of naringenin ligand motivate the test for the bathophenanthroline and the ternary complex. Bathophenanthroline did not show any activity in the 0.1–100 µM range. Nevertheless, precedent data shows that its presence in the flavonoids-metal complexes correlates with antioxidant enhancement capacity in a Cu(II)-chrysin-N-derivative ligands. (Gençkal 2020) On the contrary, the CuNarBatho acted as an efficient scavenger of superoxide radicals. This is a significant result considering that neither naringenin nor bathophenanthroline behaves as a SOD mimic per se. Data for CuNar were added for comparison purposes. However, the method used for its determination is different from that of this work.

Table 3 Free radical scavenging power (SOD mimic activity)

Compounds	IC_{50} (µM)	k_{McCF} ($mol^{-1} \times Lx\ s^{-1}$)	
SOD native	0.210	8.50×10^8	(Islas et al. 2015)
Naringenin*	> 100	$> 1.50 \times 10^5$	(Islas et al. 2015)
Naringenin**	0.262		(Wang et al. 2006)
CuNarBatho*	2.060	8.63×10^6	This work
CuNar**	0.003		(Wang et al. 2006)

*PMS/NADH/NBT system, **MET/VitB_2/NBT system

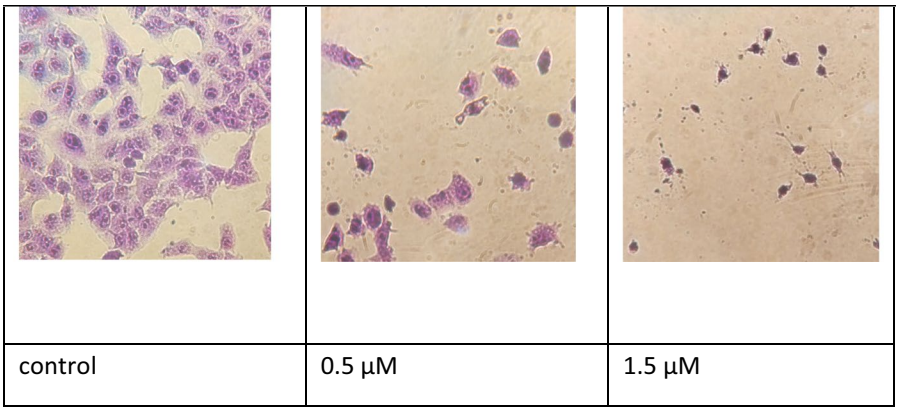

Fig. 6 Morphological changes of A549 cells after treatment with 0.5 and 1.5 µM CuNarBatho for 24 h. Control cells remained untreated and received an equal volume of the solvent (40 x)

Table 4 Effects of naringenin, bathophenanthroline, CuNarBatho, CuNar, and copper(II) cation on A549 cell viability: IC_{50} values of studied compounds and for CuNarPhen for comparative purposes

Compounds	IC_{50} (µM)
CuNarBatho	0.30 ± 0.02
CuNarPhen[#]	16.42
CuNar	> 100
Naringenin[##]	> 100
Batho	12.10 ± 2.40
Copper(II)	> 100

#$[Cu(H_2O)_2(L_1)(phen)](ClO_4)$, L_1:naringenin (Tamayo et al. 2016), [##]From Islas et al. 2015

Higher SOD activity in copper(II) complexes has been attributed to a greater interaction between the superoxide ion and the Cu(II) center in mixed-ligand-complexes due to the formation of strong axial bond. (Siddiqi et al. 2009). In the presence of Cu(II), the enhancement of this capacity has been associated with a cycle redox reaction that generates additional stabilization of the intermediates or products (Arif et al. 2018).

Anticancer activity

Cell viability To evaluate the cytotoxic activity of naringenin, bathophenanthroline, CuNar, and CuNarBatho, against the lung tumor cell line A549, an in vitro assay was carried out. As shown in Fig. 5, naringenin has minimal effects on the A549 cell viability at tested concentrations and 24 h of incubation. For naringenin, the results are following the previously published by Chang et al. and Jin et al. As previously reported, $CuCl_2$ did not show toxicity against lung cancer cells. (Martínez Medina et al. 2019).

A significant reduction in cell viability is particularly noticeable at very low concentrations of CuNarBatho being its IC_{50} value 0.3 µM. The decrease in the number of cells was confirmed by optical microscopy. After 24 h treatment with 0.5 and 1.5 µM of CuNarBatho, images of stained cells were registered (Fig. 6) and it can be observed that the complex induced cellular morphology changes typical of apoptosis: cellular shrinkage and presence of pycnotic nuclei.

For the binary complex, CuNar (Celiz et al. 2019), there was no previous data on the A549 cells. Then, for comparison purposes, the study of its anticancer activity was included. The IC_{50} value was calculated under the same conditions being greater than 100 µM (Fig. 5, Table 4). The IC_{50} value for the CuNarPhen complex (Tamayo et al. 2016) was also included to analyze a series of Cu-naringenin derivative complexes. From those results, it is evident that the increment of the complexity of the structure of the copper(II) complex (insertion of a phenanthroline based ligand) correlates with the augment of the effect on A549 cells in the following order: naringenin ~ CuNar < CuNarPhen < CuNarBatho. The addition of the phen in the coordination sphere lowers 83% of the IC_{50} value, and the inclusion of Batho instead of phen led to sub-micromolar anticancer potency.

The results confirm the data obtained by other authors who demonstrated the significance of the substitution arrangement of the phenanthroline rings is directly related to the increase of antitumor

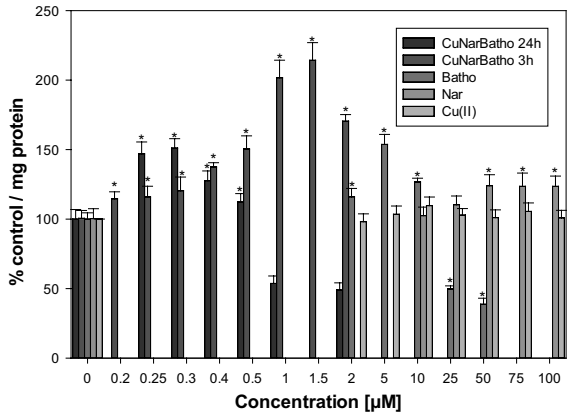

Fig. 7 Effect of naringenin, Batho, CuNarBatho and copper(II) cation on ROS production. A549 cells were incubated at 37 °C (24 h and/or 3 h) in the presence of 10 μM DCFDA which oxidizes to DCF. The values are expressed as a percentage of the control level and represent the mean ± S.E.M. *indicates significant values in comparison with the control level ($P < 0.05$)

activity of the compounds. (Celiz et al. 2019; Oliveira et al. 2017; Masuri et al. 2022).

Mechanism of action To identify the mechanisms related to the cytotoxic activity of the ternary complex, the intracellular production of reactive oxygen species (ROS), mitochondrial membrane potential disruption and GSH levels were evaluated.

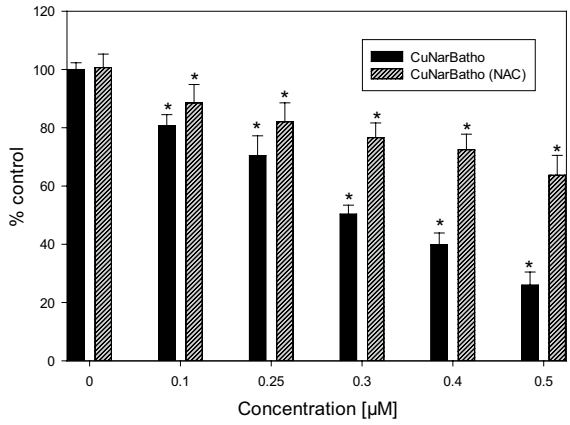

Fig. 8 Effect of N-acetyl-L-cysteine (NAC, 5 mM) on A549 cell viability induced by CuNarBatho. The values are expressed as a percentage of the control level and represent the mean ± SD. *indicates significant values in comparison with the control level ($p < 0.05$)

It is well known that flavonoids can behave as antioxidant or prooxidant substances (Procházková et al. 2011). Naringenin and some Cu(II)-complexes have been reported to be able to increase the intracellular ROS levels in different cell lines. (Ahamad et al., 2014; Ng et al. 2014; Khan et al. 2019; Lim et al. 2017) In order to evaluate intracellular ROS levels in A549 cells, the 2′,7′-dichlorofluorescein diacetate (DCFDA) assay was performed. As can be seen in Fig. 7, naringenin induced a slight increment (ca. 120%) of ROS levels above 50 μM. The ternary complex produced an increment (150% compared to control) of ROS amount up to 0.30 μM at 24 h incubation but at higher concentrations the fluorescence intensity decreased, due to an excessive cell death. At 3 h incubation, it can be observed that CuNarBatho produced an overgeneration of ROS levels (ca. 200% compared to the control) in a concentration-dependent manner up to 1.5 μM. Bathophenanthroline is capable of inducing ROS generation in the A549 cancer cells at low concentrations (up to 5 μM). Then, the fluorescence intensity decrease due to the high percentage of cell death. Copper (II) salt did not show significant differences over the untreated cells. (Martínez Medina et al. 2019).

To prove that the inhibition of A549 cancer cells produced by the ternary complex is due to ROS

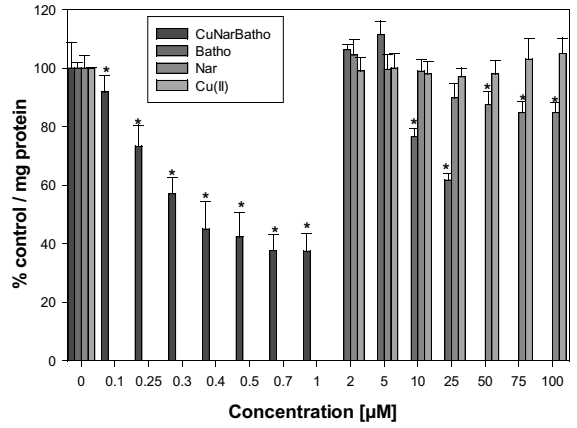

Fig. 9 Effects of naringenin, bathophenanthroline, CuNar, CuNarBatho and copper(II) cation on mitochondrial membrane potential (ΔΨm) in lung cancer cells. A549 cells were treated with DMSO (control) or compounds for 24 h. Mitochondrial membrane potential was measured by $DIOC_6$ staining and analyzed by fluorescence spectroscopy. The data shown are mean ± S.E.M of triplicate samples for each treatment. *$p < 0.05$ compared with control

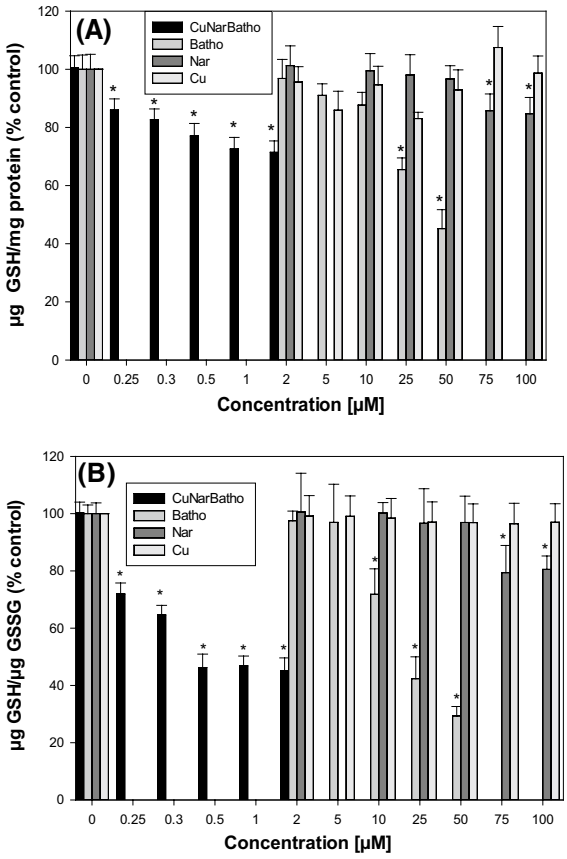

Fig. 10 Effects of naringenin, bathophenanthroline, CuNarBatho and copper(II) cation on GSH cellular levels (A) and GSH/GSSG ratio (B) in A549 cells. Results are expressed as mean ± SEM of three independent experiments, *significant differences in comparison with the control level ($p < 0.05$)

generation, the cells were treated with the antioxidant NAC (N-acetylcysteine). Although preincubation with 5 mM NAC did not fully restore cell viability, the CuNarBatho-induced less growth inhibition in A549 cells indicating that ROS are involved in the cell death pathway (see Fig. 8).

The mitochondrial dysfunction is associated with malignant cell transformation. In healthy cells, a high mitochondrial membrane potential ($\Delta\Psi m$) is critical for maintaining the physiological function of the respiratory chain to generate ATP. However, in cancer cells, a significant loss of $\Delta\Psi m$ is related to the loss of cellular energy leading to subsequent cell death by apoptosis (Ly et al. 2003). To test the effect of compounds on $\Delta\Psi m$, cationic lipophilic fluorescent dye $DIOC_6$, which accumulates specifically in the mitochondria of living cells, was employed. As Fig. 9 illustrated, naringenin induced a slight reduction of mitochondrial membrane potential (*ca*.15% at 100 µM). A significant reduction in fluorescence intensity compared to the control cells was observed when A549 cells were incubated with CuNarBatho and Bathophenanthroline (ca. 60% at 1 µM and 40% at 25 µM, respectively). Overall the results suggested that treatment of A549 cells with ligands and complex can induce apoptosis mediated by the disruption of the mitochondrial membrane potential.

The tripeptide, γ-l-glutamyl-l-cysteinyl-glycine known as glutathione (GSH, reduced glutathione) is the most important low molecular weight antioxidant in all mammalian cell types. GSH plays a critical role in various biological processes, among them, it protects cells from oxidative injury and maintains redox homeostasis. GSH ratio with oxidized glutathione (GSSG) may be used as a marker of oxidative stress (Jay Forman et al. 2009) The results of depletion in the GSH levels in cultured A549 cells exposed to compounds for 24 h are shown in Fig. 10. GSH level and GSH/GSSG ratio were reduced after treatment with increasing concentration of CuNarBatho (ca. 30 and 60% respectively). Bathophenanthroline induced depletion of GSH level and GSH/GSSG ratio above 10 µM concentration and naringenin above 75 µM. Naringenin reduced both parameters to a lesser extent (*ca*. 15%). Copper(II) did not show a significant difference with the untreated cells (Naso et al. 2020).

Naringenin slightly inhibited cell viability at high concentrations. Lu et al. (Lu et al. 2020) found that the free ligand induces apoptosis by activating mitochondrial pathway above 200 µM. In our previous work, (Islas et al. 2015) no cytotoxic effect of naringenin on the A549 cell viability was found up to a concentration of 100 µM. In this work we showed that the flavonoid exert a weak effect on the tested parameters, ROS generation, GSH levels, and mitochondrial membrane potential disruption.

Tamayo et al. found that CuNarPhen showed a reductive stress action with reduction of ROS production and acted by a mitochondria-independent apoptotic mechanism.

The results of this work indicate that cell death induced by CuNarBatho is related to an oxidative stress with ROS production at short exposure time, loss of mitochondrial membrane potential, and depletion of GSH level and GSH/GSSG ratio. A similar

mechanism of action was found to METVAN (A549) (D'Cruz et al. 2002) and casiopeinas (Casiopeina II-gly (Cas IIgly), glioma C6 cells) (Trejo-Solís et al. 2005). Surprisingly, the IC_{50} value of CuNarBatho is 70 times lower than IC_{50} of cisplatin (Al Hageh et al. 2018) suggesting that the complex is a promising candidate for further biological studies.

This study demonstrated that structural differences led to a very different anticancer ability and different mechanisms of action. It is known that a cytotoxic action can be exerted by different mechanisms. The prevalence of one or more of them depends on multiple factors. (Masuri et al. 2022) Additional studies in future work would be convenient to evaluate other involving factors.

Conclusions

The complex CuNarBatho was synthesized and fully characterized by several physicochemical techniques as elemental analysis, molar conductivity, mass spectrometry, thermogravimetric measurements and UV–VIS, FT-IR, Raman, EPR and ^{1}H-NMR spectroscopies. These results indicate that the solid copper(II) complex is dimeric. The coordination around the copper(II) ion occurs via naringenin binding (through the deprotonated C5 hydroxyl group and the C4 = O group), bathophenanthroline binding (by the N-atoms) and chloride ions. The complex enhances the effect of naringenin on the dismutation of superoxide radicals. Its *kMcCF*-constant value is almost 10^4 times more effective than the ligand. Albumin binding experiments show the possibility of a reversible type of binding with a K_b constant greater than naringenin. Thermodynamic parameters suggest an enthalpic-driven process including Van der Walls and H-bond formation. Thus, the complex could be reversible transported by albumin.

Anticancer activity of naringenin, CuNar, and CuNarBatho complexes showed that only the ternary complex exhibited an antiproliferative effect on A549 cells. Superior anticancer action was found for the CuNarBatho complex with a different mechanism of action than CuNarPhen associated with the production of ROS, the loss of the mitochondrial membrane potential, and the depletion of GSH level and GSH/GSSG ratio.

This study supports the potential of copper(II)-phenanthroline complexes as anticancer drugs based on the chemical advantages of Cu(II) cation (different coordination numbers and geometries, diverse types of ligands), and the involvement of the structural complexity of the substituted phenanthroline that increases the anticancer potency in comparison with other N,N-ligands derivatives.

Acknowledgements This work was supported by Agencia Nacional de Promoción Científica y Tecnológica (ANPCyT-PICT-2019-00945), Consejo Nacional de Investigaciones Científicas y Técnicas (CONICET-PIP1999- 2021-2023), PUE-22920170100053CO (CONICET) and Universidad Nacional de La Plata (UNLP-X777), Argentina. LGN, EGF, M.G.R and P.J.G. are members of the Research Career, CONICET, Argentina. PAMW is member of the Research Career, CICPBA. J.C.R. is fellowship holder from CONICET.

Authors contribution Conceptualization: PAMW, LGN, EGF. Methodology: JYC-R, LGN, MGR, PJG. Validation: PAMW, LGN, EGF. Formal analysis: JYC-R, LGN, MGR, PJG. Investigation: JYC-R, LGN, MGR, PJG. Resources: PAMW, EGF. Writing e original draft: LGN, EGF. Writing e review and editing: PAMW, LGN, EGF. Visualization: LGN, EGF. Supervision: PAMW, LGN, EGF. Project administration: PAMW, EGF. Funding acquisition: PAMW, EGF. The authors have no competing interests to declare that are relevant to the content of this article.

References

Aboukais A, Bennani A, Aissi C, Wrobel G, Guelton M, Vedrine JC (1992) Highly resolved electron paramagnetic resonance spectrum of copper(II) ion pairs in CuCe oxide. J Chem Soc, Faraday Trans 88:615–620. https://doi.org/10.1039/FT9928800615

Ahamad MS, Siddiqui S, Jafri A, Ahmad S, Afzal M, Arshad M (2014) Induction of apoptosis and antiproliferative activity of naringenin in human epidermoid carcinoma cell through ROS generation and cell cycle arrest. PLoS ONE 9:e110003. https://doi.org/10.1371/journal.pone.0110003

Akkoç Y, Berrak O, Arısan E, Obakan P, Çoker-Gurkan A, Palavan-Unsal N (2015) Inhibition of PI3K signaling triggered apoptotic potential of curcumin which is hindered by Bcl-2 through activation of autophagy in MCF-7 cells. Biomed Pharmacother 71:161–171. https://doi.org/10.1016/j.biopha.2015.02.029

Al Hageh C, Al Assaad M, El Masri Z, Samaan N, El-Sibai M, Khalil C, Khnayzer RS (2018) A long-lived cuprous bis-phenanthroline complex for the photodynamic therapy of cancer. Dalton Trans 47:4959–4967. https://doi.org/10.1039/C8DT00140E

Arif H, Sohail A, Farhan M, Rehman AA, Ahmad A, Hadi SM (2018) Flavonoids-induced redox cycling of copper ions leads to generation of reactive oxygen species: a potential role in cancer chemoprevention. Int J Biol Macromol 106:569–578. https://doi.org/10.1016/j.ijbiomac.2017.08.049

Bi S, Yan L, Pang B, Wang Y (2012) Investigation of three flavonoids binding to bovine serum albumin using molecular

fluorescence technique. J Lumin 132:132–140. https://doi.org/10.1016/j.jlumin.2011.08.014

Bradford MM (1976) A rapid and sensitive method for the quantitation of microgram quantities of protein utilizing the principle of protein-dye binding. Anal Biochem 72:248–254. https://doi.org/10.1016/0003-2697(76)90527-3

Calvo R, Santana VT (2017) Temperature dependence of the effective interdimer exchange interaction in a weakly coupled antiferromagnetic dimer copper compound. Physl Rev B 96:064424. https://doi.org/10.1103/PhysRevB.96.064424

Celiz G, Suarez SA, Arias A, Molina J, Brondino CD, Doctorovich F (2019) Synthesis, structural elucidation and antiradical activity of a copper (II) naringenin complex. Biometals 32:595–610. https://doi.org/10.1007/s10534-019-00187-3

Chang H, Chang Y, Lai S, Chen K, Wang K, Chiu T, Chang F, Hsu L (2017) Naringenin inhibits migration of lung cancer cells via the inhibition of matrix metalloproteinases-2 and -9. Exp Ther Med 13:739–744. https://doi.org/10.3892/etm.2016.3994

D'Cruz JO, Uckun FM, Fatih M (2002) Metvan: a novel oxovanadium(IV) complex with broad spectrum anticancer activity. Expert Opin Investig Drugs 11:1829–1836. https://doi.org/10.1517/13543784.11.12.1829

Dasari S, Tchounwou PB (2014) Cisplatin in cancer therapy: molecular mechanisms of action. Eur J Pharmacol 740:364–378. https://doi.org/10.1016/j.ejphar.2014.07.025

Eaton SS, More KM, Sawant BM, Eaton GR (1983) Use of the ESR half-field transition to determine the interspin distance and the orientation of the interspin vector in systems with two unpaired electrons. J Am Chem Soc 105:6560–6567. https://doi.org/10.1021/ja00360a005

Filho JCC, Franceschini Sarria AL, Blanque Becceneri A, Fuzer AM, Batalhao JR, Paranhos da Silva CM, Carlos RM, Vieira PC, Fernandes JB, Cominetti MR (2014) Copper (II) and 2,2'-bipyridine complexation improves chemopreventive effects of naringenin against breast tumor cells. PLoS One 9:e107058. https://doi.org/10.1371/journal.pone.0107058

Gençkal HM (2020) New heteroleptic Cu(II) complexes of chrysin with 2,2 bipyridine and substituted 1,10ephenanthrolines: synthesis, characterization, thermal stability and antioxidant activity. J Mol Struc 1209:127917. https://doi.org/10.1016/j.molstruc.2020.127917

Gibson GTT, Mohamed MF, Neverov AA, Brow RS (2006) Potentiometric titration of metal ions in ethanol. Inorg Chem 45:7891–7902. https://doi.org/10.1021/ic060517x

Hissin PJ, Hilf R (1976) A fluorometric method for determination of oxidized and reduced glutathione in tissues. Anal Biochem 74:214–226. https://doi.org/10.1016/0003-2697(76)90326-2

Islas MS, Naso LG, Lezama L, Valcarcel M, Salado C, Roura-Ferrer M, Ferrer EG, Williams PAM (2015) Insights into the mechanisms underlying the antitumor activity of an oxidovanadium(IV) compound with the antioxidant naringenin. Albumin Binding Studies J Inorg Biochem 149:12–24. https://doi.org/10.1016/j.jinorgbio.2015.04.011

Jay Forman H, Zhang H, Rinna A (2009) Glutathione: Overview of its protective roles, measurement, and biosynthesis. Mol Aspects Med 30:1–12. https://doi.org/10.1023/a:10.1016/j.mam.2008.08.006

Jin C, Park C, Hwang HJ, Kim G, Choi BT, Kim W, Choi YH (2011) Naringenin up-regulates the expression of death receptor 5 and enhances TRAIL-induced apoptosis in human lung cancer A549 cells. Mol Nutr Food Res 55:300–309. https://doi.org/10.1002/mnfr.201000024

Joseph M, Kuriakose M, Prathapachandra Kurup MR, Suresh E, Kishore A, Bhat SG (2006) Structural, antimicrobial and spectral studies of copper(II) complexes of 2-benzoylpyridine N(4)-phenyl thiosemicarbazone. Polyhedron 25:61–70. https://doi.org/10.1016/j.poly.2005.07.006

Khan MH, Cai M, Deng J, Yu P, Liang H, Yang F (2019) Anticancer function and ROS-mediated multi-targeting anticancer mechanisms of Copper(II) 2-hydroxy-1-naphthaldehyde complexes. Molecules 24:2544–2564. https://doi.org/10.3390/molecules24142544

Lakowicz JR (2013) Principles of fluorescence spectroscopy. Springer Science & Business Media, New York

Lim W, Park S, Bazer FW, Song GJ (2017) Naringenin-induced apoptotic cell death in prostate cancer cells is mediated via the PI3K/AKT and MAPK signaling pathways. J Cell Biochem 118:1118–1131. https://doi.org/10.1002/jcb.25729

Ling L, Tan K, Lin H, Chiu G (2011) The role of reactive oxygen species and autophagy in safingol-induced cell death. Cell Death Dis 2:e129. https://doi.org/10.1038/cddis.2011.12

Litos C, Parsons S, Karaliota A (2007) Synthesis of two dicopper(II) complexes of L-carnitine: the first structural determination of a metal complex containing L-carnitine. Polyhedron 26:1397–1403. https://doi.org/10.1016/j.poly.2006.11.010

Lu W-L, Ricky Yu C-T, Lien H-S, Sheu G-T, Cherng S-H (2020) Cytotoxicity of naringenin induces Bax-mediated mitochondrial apoptosis in human lung adenocarcinoma A549 cells. Environ Toxicol 35:1386–1394. https://doi.org/10.1002/tox.23003

Ly JD, Grubb DR, Lawen A (2003) The mitochondrial membrane potential (Δψm) in apoptosis; an update. Apoptosis 8:115–128. https://doi.org/10.1023/a:1022945107762

Mahmud KM, Niloy MS, Shakil MS, Islam MA (2021) Ruthenium complexes: an alternative to platinum drugs in colorectal cancer treatment. Pharmaceutics 13:1295–1325. https://doi.org/10.3390/pharmaceutics13081295

Martínez Medina JJ, Naso LG, Pérez AL, Rizzi A, Okulik NB, Valcarcel M, Salado C, Ferrer EG, Williams PAM (2019) Synthesis, characterization, theoretical studies and biological (antioxidant, anticancer, toxicity and neuroprotective) determinations of a copper(II) complex with 5-hydroxytryptophan. Biomed Pharmacother 111:414–426. https://doi.org/10.1016/j.biopha.2018.12.098

Masuri S, Vaňhara P, Cabiddu MG, Moráň L, Havel J, Cadoni E, Pivetta T (2022) Copper(II) phenanthroline-based complexes as potential anticancer drugs: a walkthrough on the mechanisms of action. Molecules 27:49. https://doi.org/10.3390/molecules27010049

Mosae Selvakumar P, Nadella S, Sahoo J, Suresh E, Subramanian PS (2013) Copper(II) bis-chelate paddle wheel

complex and its bipyridine/phenanthroline adducts. J Coord Chem 66:287–299. https://doi.org/10.1080/00958972.2012.755521

Nan Z, Hao C, Ye X, Feng Y, Sun R (2019) Interaction of graphene oxide with bovine serum albumin: a fluorescence quenching study. Spectrochim Acta Part A 210:348–354. https://doi.org/10.1016/j.saa.2018.11.028

Naso LG, Martínez Medina JJ, D'Alessandro F, Rey M, Rizzi A, Piro OE, Echeverría GA, Ferrer EG, Williams PAM (2020) Ternary copper(II) complex of 5-hydroxytryptophan and 1,10- phenanthroline with several pharmacological properties and an adequate safety profile. J Inorg Biochem 204:110933. https://doi.org/10.1016/j.jinorgbio.2019.110933

Ng CH, Kong SM, Tiong YL, Maah MJ, Sukram N, Ahmade M, Khoo ASB (2014) Selective anticancer copper(ii)-mixed ligand complexes: targeting of ROS and proteasomes. Metallomics 6:892–906. https://doi.org/10.1039/C3MT00276D

Oliveira KM, Liany L-D, Corrêa RS, Deflon VM, Cominetti MR, Batista AA (2017) Selective Ru(II)/lawsone complexes inhibiting tumor cell growth by apoptosis. J Inorg Biochem 176:66–76. https://doi.org/10.1016/j.jinorgbio.2017.08.0

Patel K, Singh GK, Patel DK (2018) A review on pharmacological and analytical aspects of naringenin. Chin J Integr Med 24:551–560. https://doi.org/10.1007/s11655-014-1960-x

Peisach J, Blumberg WE (1974) Structural implications derived from the analysis of electron paramagnetic resonance spectra of natural and artificial copper proteins. Arch Biochem Biophys 165:691–708. https://doi.org/10.1016/0003-9861(74)90298-7

Pereira RMS, Andrades NED, Paulino N, Sawaya ACHF, Eberlin MN, Marcucci MC, Favero GM, Novak EM, Bydlowski SP (2007) Synthesis and characterization of a metal complex containing naringin and Cu, and its antioxidant. Antimicrob Antiinflam Tumor Cell Cytotoxicity Mol 12:1352–1366. https://doi.org/10.3390/12071352

Procházková D, Boušová I, Wilhelmová N (2011) Antioxidant and prooxidant properties of flavonoids. Fitoterapia 82:513–523. https://doi.org/10.1016/j.fitote.2011.01.018

Ramos PM, Pereira Silva PS, Chamorro-Posada P, Ramos Silva M, Milne BF, Nogueira F, Martín-Gil J (2014) Synthesis, structure, theoretical studies and luminescent properties of a ternary erbium(III)complex with acetylacetone and bathophenanthroline ligands. J Lumin 162:41–49. https://doi.org/10.1016/j.jlumin.2015.02.024

Rizzi AC, Neuman NI, González PJ, Brondino CD (2016) EPR as a tool for study of isolated and coupled paramagnetic centers in coordination compounds and macromolecules of biological interest. Eur J Inorg Chem 2:192–207. https://doi.org/10.1002/ejic.201690002

Ruiz-Azuara L, Bastian G, Bravo-Gómez ME, Cañas RC, Flores-Alamo M, Fuentes I, Mejia C, García-Ramos J, Serrano A (2014) Abstract CT408: phase I study of one mixed chelates copper(II) compound, Casiopeína CasIIIia with antitumor activity and its mechanism of action. AACR Cancer Res 74(Suppl 19):CT408. https://doi.org/10.1158/1538-7445.AM2014-CT408

Shahabadi N, Falsafi M, Moghadam N (2013) DNA interaction studies of a novel Cu(II) complex as an intercalator containing curcumin and bathophenanthroline ligands. J Photochem Photobiol B: Biology 122:45–51. https://doi.org/10.1021/10.1016/j.jphotobiol.2013.03.002

Siddiqi ZA, Shahid M, Khalid M, Kumar S (2009) Antimicrobial and SOD activities of novel transition metal ternary complexes of iminodiacetic acid containing a-diimine as auxiliary ligand. Eur J Med Chem 44:2517–2522. https://doi.org/10.1016/j.ejmech.2009.01.025

Stoll S, Schweiger A (2006) EasySpin, a comprehensive software package for spectral simulation and analysis in EPR. J Magn Reson 178:42–55. https://doi.org/10.1016/j.jmr.2005.08.013

Sung H, Ferlay J, Siegel RL, Laversanne M, Soerjomataram I, Jemal A, Bray F (2021) Global cancer statistics 2020: GLOBOCAN estimates of incidence and mortality worldwide for 36 cancers in 185 countries. CA-Cancer J Clin 71:209–249. https://doi.org/10.3322/caac.21660

Tamayo LV, Gouvea LR, Sousa AC, Albuquerque RM, Fernandes Teixeira S, de Azevedo RA, Louro SRW, Kleber Ferreira A, Beraldo H (2016) Copper(II) complexes with naringenin and hesperetin: cytotoxic activity against A 549 human lung adenocarcinoma cells and investigation on the mode of action. Biometals 29:39–52. https://doi.org/10.1007/s10534-015-9894-0

Tan M, Zhu J, Pan Y, Chen Z, Liang H, Liu H, Wang H (2009) Synthesis, cytotoxic activity, and DNA binding of copper (II) complexes with Hesperetin. Naringenin, and Apigenin Bioinorg Chem App. https://doi.org/10.1155/2009/347872

Teipel S, Griesar K, Haase W, Krebs B (1994) A New Type of.mu.4-Oxo-bridged copper tetramer: synthesis, x-ray molecular structure, magnetism and spectral properties of (.mu.4-Oxo)tetrakis(.mu.-bromo)bis(.mu.-2,6-bis(morpholinomethyl)-4-methylphenolato) tetracopper(II) and (.mu.4-Oxo)tetrakis(.mu.-benzoato) bis(.mu.-2,6-bis(morpholinomethyl)-4-methylphenolato) tetracopper(II). Inorg Chem 33:456–464. https://doi.org/10.1021/ic00081a011

Uivarosi V, Munteanu A-C (2017) Flavonoid complexes as promising anticancer metallodrugs. In: Justino J (ed) Flavonoids-from biosynthesis to human health. InTech

Vančo J, Trávníček Z, Hošek J, Malina T, Dvořák Z (2021) Copper(II) complexes containing natural flavonoid pomiferin show considerable in vitro cytotoxicity and anti-inflammatory effects. Int J Mol Sci 22:7626–7652. https://doi.org/10.3390/ijms22147626

Wang H-L, Yang Z-Y, Wang B-d (2006) Synthesis, characterization and the antioxidative activity of copper(II), zinc(II) and nickel(II) complexes with naringenin. Transit Met Chem 31:470–474. https://doi.org/10.1007/s11243-006-0015-3